

Calibration of Temperature Related WFC3 IR Dark Current Variations

B. Hilbert, M. Robberto
December 15, 2005

ABSTRACT

The 2004 thermal vacuum campaign to test the WFC3-IR channel revealed dark current rates that were highly correlated with the temperature of FPA64. Using the inboard reference pixels, we have explored a calibration method that successfully removes these temperature effects in all but the shortest sample sequences. This correction should become part of the IR channel's standard data processing pipeline.

Introduction

Previous dark current behavior studies of the WFC3 IR channel revealed a temperature related variation in the dark current rate (Hilbert and Robberto, 2005). Small (0.3°C) drifts in detector temperature were associated with changes in the IR dark rate by up to 70%. While a hardware fix to correct this problem is under study, we have explored possible ways to compensate for these effects in software, using the reference pixels present on the 5 outer rows and columns of FPA64. For a description of the reference pixels on the IR FPA, see Robberto et al. 2002.

Data

Ramps used in the development and testing of this new dark current calibration strategy include dark current files taken in the IR01S03, IR01S04, and IR01S05 SMSs during 2004 thermal vacuum testing. These data monitored the dark current in the IR channel at

FPA temperatures within 1°C of nominal temperature (150K) using exposure times from 64 seconds to 2,800 seconds. These data are listed in Table 1.

SMS	Sample Sequence	Files	
IR01S03	SPARS200	ii01030rr_04251223044_raw.fits	
		ii01030tr_04251231753_raw.fits	
		ii01030vr_04252000530_raw.fits	
		ii01030rr_04262133149_raw.fits	
		ii01030tr_04262141858_raw.fits	
		ii01030vr_04262150635_raw.fits	
	SPARS100	ii01030nr_04251211346_raw.fits	
		SPARS50	ii01030ir_04251201401_raw.fits
	SPARS25	ii01030br_04267115235_raw.fits	
	RAPID	ii010301r_04262094311_raw.fits	
		ii010301r_04267092213_raw.fits	
		ii010301r_04267105713_raw.fits	
	IR01S04	STEP400	ii01040nr_04252042138_raw.fits
			ii01040pr_04252050844_raw.fits
ii01040sr_04252060219_raw.fits			
ii01040nr_04262192143_raw.fits			
ii01040pr_04262200849_raw.fits			
ii01040sr_04262210224_raw.fits			
STEP200		ii01040kr_04262180724_raw.fits	
STEP100		ii01040dr_04262165141_raw.fits	
STEP50		ii010407r_04262160557_raw.fits	
STEP25		ii010402r_04262153217_raw.fits	
IR01S05	MIF1500	ii01050ir_04252130713_raw.fits	
		ii01050ir_04252174913_raw.fits	
		ii01050kr_04252133238_raw.fits	
		ii01050mr_04252135831_raw.fits	
		ii01050ir_04263001317_raw.fits	
		ii01050kr_04263003842_raw.fits	
		ii01050mr_04263010435_raw.fits	
		MIF600	ii010501r_04252081632_raw.fits
	ii010501r_04252102133_raw.fits		
	ii010501r_04252150333_raw.fits		
	ii010501r_04262212737_raw.fits		

Table 1. Files used to create the calibration of the temperature-dependent dark current variation.

Analysis

Prior to data analysis, all files were run through the IDL data processing pipeline detailed in Hilbert, 2004. Reference pixels were used to provide bias correction, and the zeroth read was subtracted from all subsequent reads of a given ramp, as a KTC noise correction. Finally, cosmic rays were identified and corrected, and hot/dead pixels were masked using the most recent bad pixel mask.

Detector Behavior

Examination of both inboard and outboard reference pixels revealed that the inboard reference pixels were more effective at tracking the temperature-sensitive effects observed in the science pixels. Figure 1 below shows the median signal measured in the quadrant 1 inboard reference pixels during a 2,800 second exposure, along with the FPA temperature during the exposure. The corresponding quadrant 1 median signal in the active pixels is shown in Figure 2. For both active and reference pixels, there is a sinusoidal variation in signal, which in the case of the active pixels is superimposed upon the straight line of the constant dark current rate. The relation between the sinusoidal signal variation and the detector temperature is also apparent.

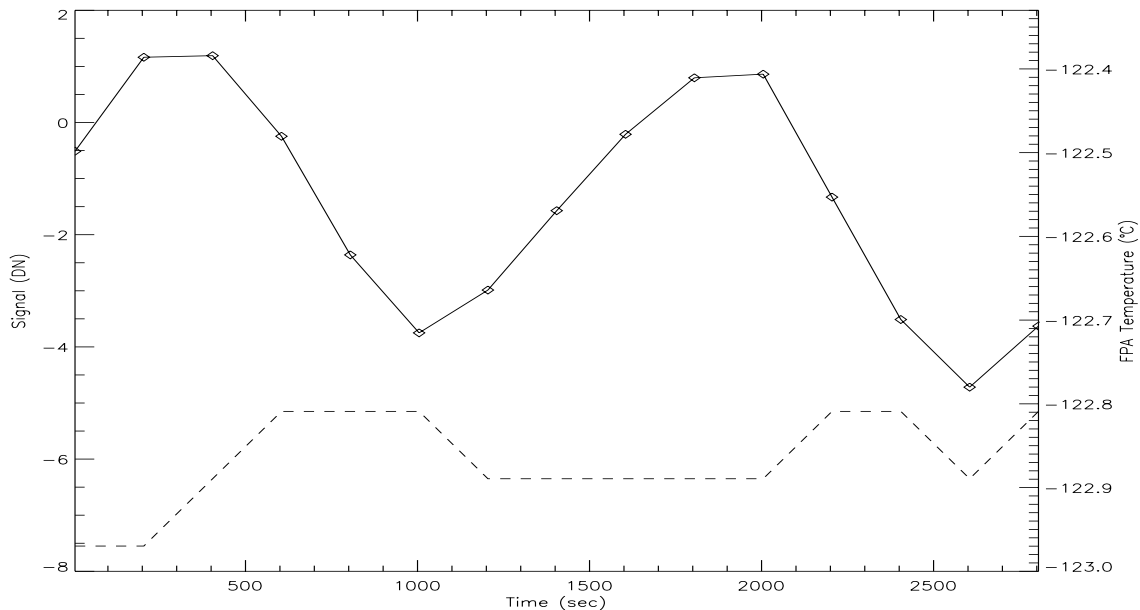


Figure 1: Reference pixel signal (solid line) and FPA temperature (dashed line) during a SPARS200 ramp taken during thermal vacuum testing. The cyclical signal observed in the reference pixels was similar to that seen in the active pixels.

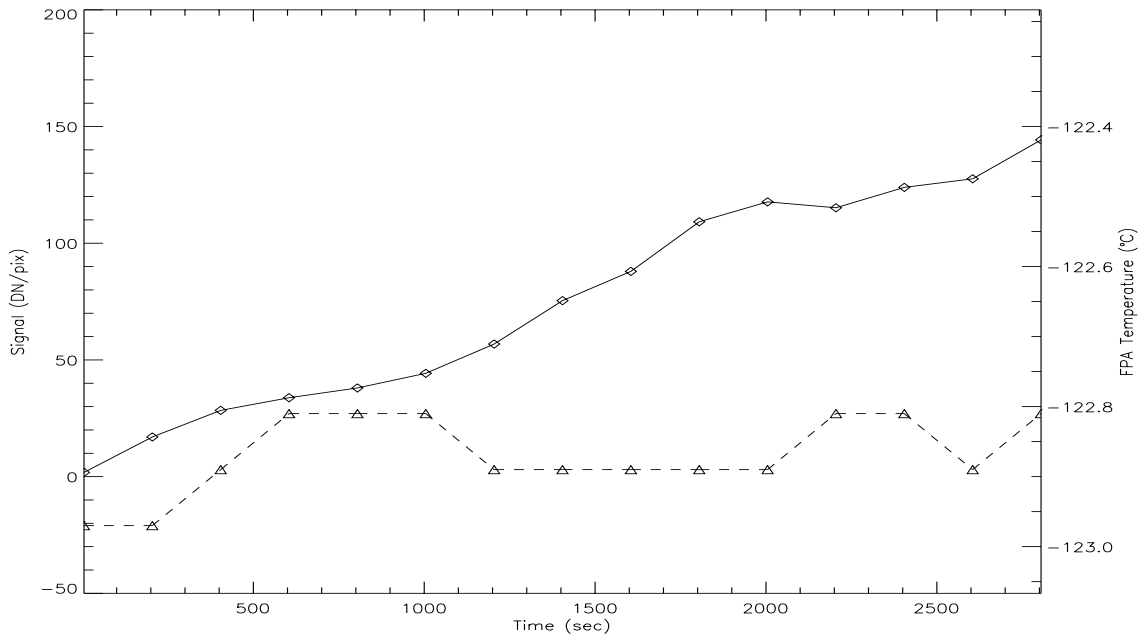


Figure 2: Median signal (solid line) and FPA temperature (dashed line) in the quadrant 1 active pixels during a SPARS200 exposure.

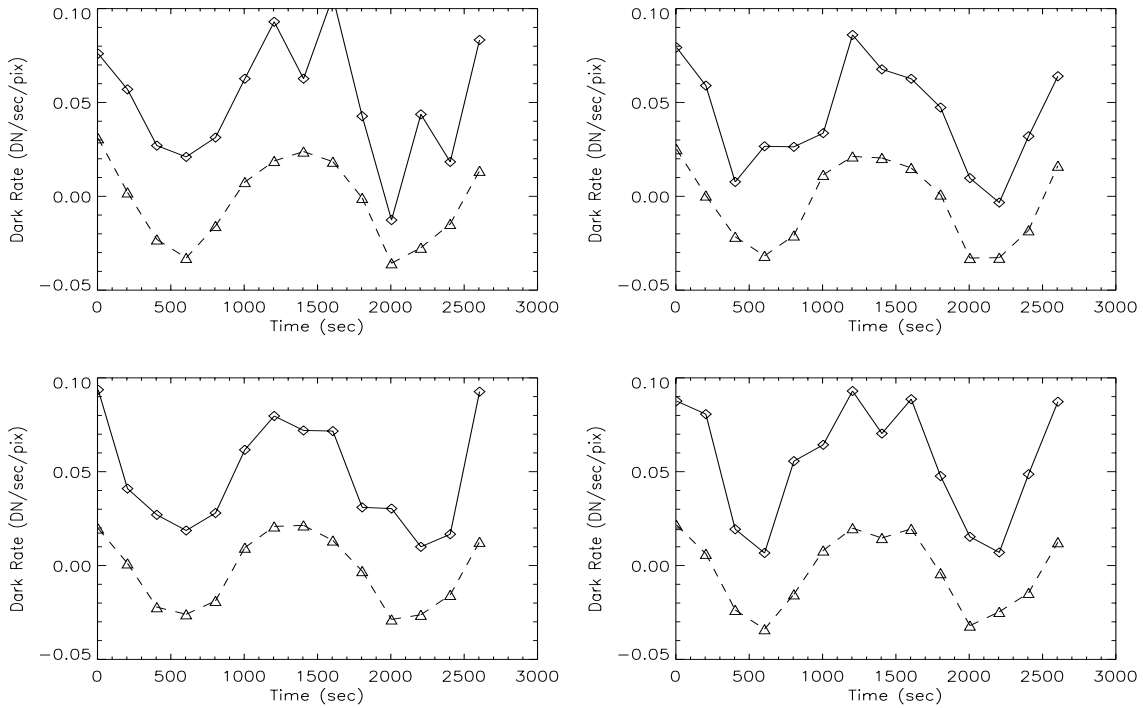


Figure 3: Signal differences between reads for a SPARS200 ramp. The solid line shows the median signal rate for the active pixels in each quadrant, while the dashed line shows the same for the inboard reference pixels, multiplied by 3 in order to facilitate comparison.

A direct comparison of active and reference pixel behavior is shown in Figure 3, where the signal rates (i.e. with the linear dark current ramp component removed) for the two types of pixels are plotted together. The correlation between the signal rates suggests that the proper subtraction of the reference pixel signals from the active pixel signals may be able to remove the temperature effects from the measured signal.

Calibration method

In order to remove the temperature related variations in dark current from the active pixels, the signal in the inboard reference pixels was used. The amplitude of the signal variation up the ramp in the reference pixels was smaller than that of the active pixels, as seen in Figure 3. As a result, the reference pixel signal had to be scaled up to match the observed variations in the active pixel signals.

An appropriate scale factor was calculated for each quadrant using the SPARS200 and STEP400 files from the IR01S03 and IR01S04 tests during the 2004 thermal vacuum testing. Each of these 12 ramps each has an exposure time of 2,800 seconds, which was long enough to sample roughly two cycles of the dark current oscillation. For each of the 15 reads within these 12 ramps, we calculated corresponding median signals in the active and reference pixels. Median rates were calculated from the median signals. We then fit a line to the rate in the active pixels versus that in the reference pixels using the rates from all 12 ramps, as shown in Figure 4. The slope of this line is ideally the ratio of the gain of the active versus reference pixels of the IR channel.

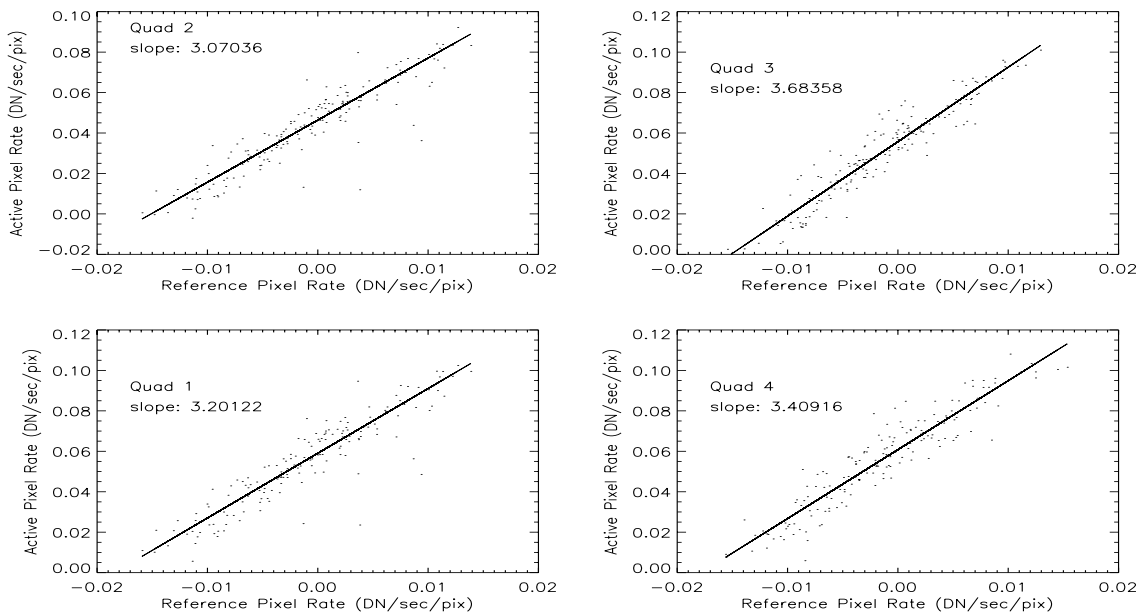


Figure 4: Plots of quadrant-averaged science pixel signal rate versus reference pixel signal rate, along with best-fit line. The slope of the line is the effective gain between the reference pixels and active pixels of the IR channel. Reference pixels were multiplied by these gain values to scale them to the active pixel signal levels.

Quad 1	Quad 2	Quad 3	Quad 4
3.20 +/- 0.08	3.07 +/- 0.07	3.68 +/- 0.10	3.41 +/- 0.10

Table 2. Slopes for each quadrant of the plots shown in Figure 4. Uncertainties listed are the 1σ uncertainties in the slope of the fit.

$$(1) \quad \textit{scaled_ref} = \textit{gain} * (\textit{ref} - \textit{mean}(\textit{ref}))$$

$$(2) \quad \textit{fixed_active} = \textit{active} - \textit{scaled_ref}$$

These slopes, one for each quadrant of FPA64 (Table 2), can be used to remove the temperature effects from other FPA64 ramps. Equations 1 and 2 detail the method used to correct the signal in the active pixels of a ramp. Each variable (except *gain*) in Equations (1) and (2) represents an array, with a length equal to the number of reads in the ramp. The *ref* and *scaled_ref* arrays represent the quadrant-wide median reference pixel signals before and after scaling by the gain (from Table 2), respectively. *active* and *fixed_active* represent the signal in a single active pixel before and after reference pixel subtraction, respectively. Equation (1) is applied once per quadrant, while Equation (2) is used once for each active pixel in the ramp being corrected.

Subtracting the mean value in Equation (1), we constrain the reference pixel signals to vary about zero. This was found to provide the best calibration for long, well-sampled ramps. For short exposures or sparsely sampled ramps, the mean value may be biased to the higher or lower signal values in the oscillation. In these cases it may be more appropriate to subtract an absolute, temperature-dependent constant that has been previously determined.

Quadrant-averaged results from this subtraction for a SPARS200 ramp are shown in Figures 5 and 6. The calibration successfully removed the sinusoidal variation seen in the original data.

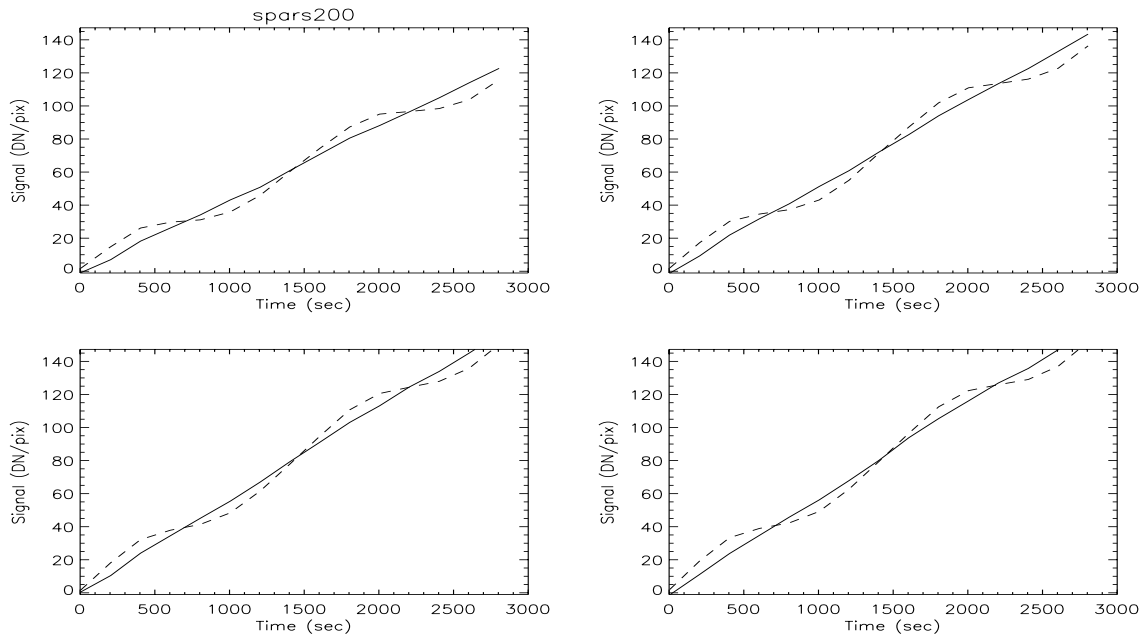


Figure 5: Quadrant-averaged signals for a SPARS200 ramp. The uncalibrated median signals in the active pixels are shown as dashed lines, while the signals measured after the reference pixel subtraction are shown as solid lines. The uncorrected signals differed from linear by up to 15%, while the corrected signals are linear to within 2%

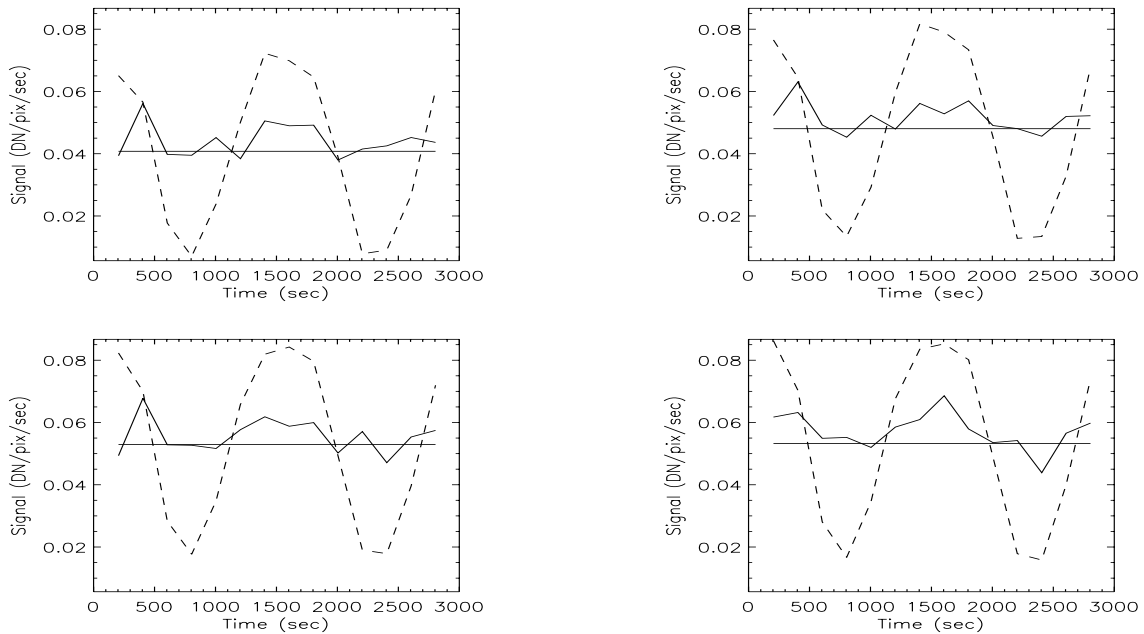


Figure 6: Same results as shown in Figure 5, but plotted in signal rates rather than signal. The dashed line gives the uncorrected rates, while the solid line shows the rates after calibration. Original rates varied about the median dark rate by up to 66%, while the corrected rates are linear to within 15%

Figures 7 through 10 show the results of the calibration when applied to data taken with other sample sequences and on different days. These figures show that the temperature-related dark current variations are effectively removed, leaving a linear dark current signal, in all but the shortest sample sequences (SPARS25, STEP25, RAPID, exposure times $< \sim 300$ seconds). The corrected signals in the short sample sequences (Figure 10) are often more noisy and at times, less linear, than the uncorrected signals.

For long ($> \sim 500$ seconds) sample sequences, the calibration removes the observed cyclical variations, leaving behind a linear dark current rate.

With the observed temperature-induced variations having a period of $\sim 1,500$ seconds, intermediate length exposures ($\sim 300 - 600$ seconds) are not long enough to clearly display the sinusoidal variations in dark current. Instead, dark current variations are manifested as linear, non-nominal dark current rates (Figure 7, bottom panels, and Figure 9, MIF600 panels). Our calibration rescales these dark currents to the nominal level.

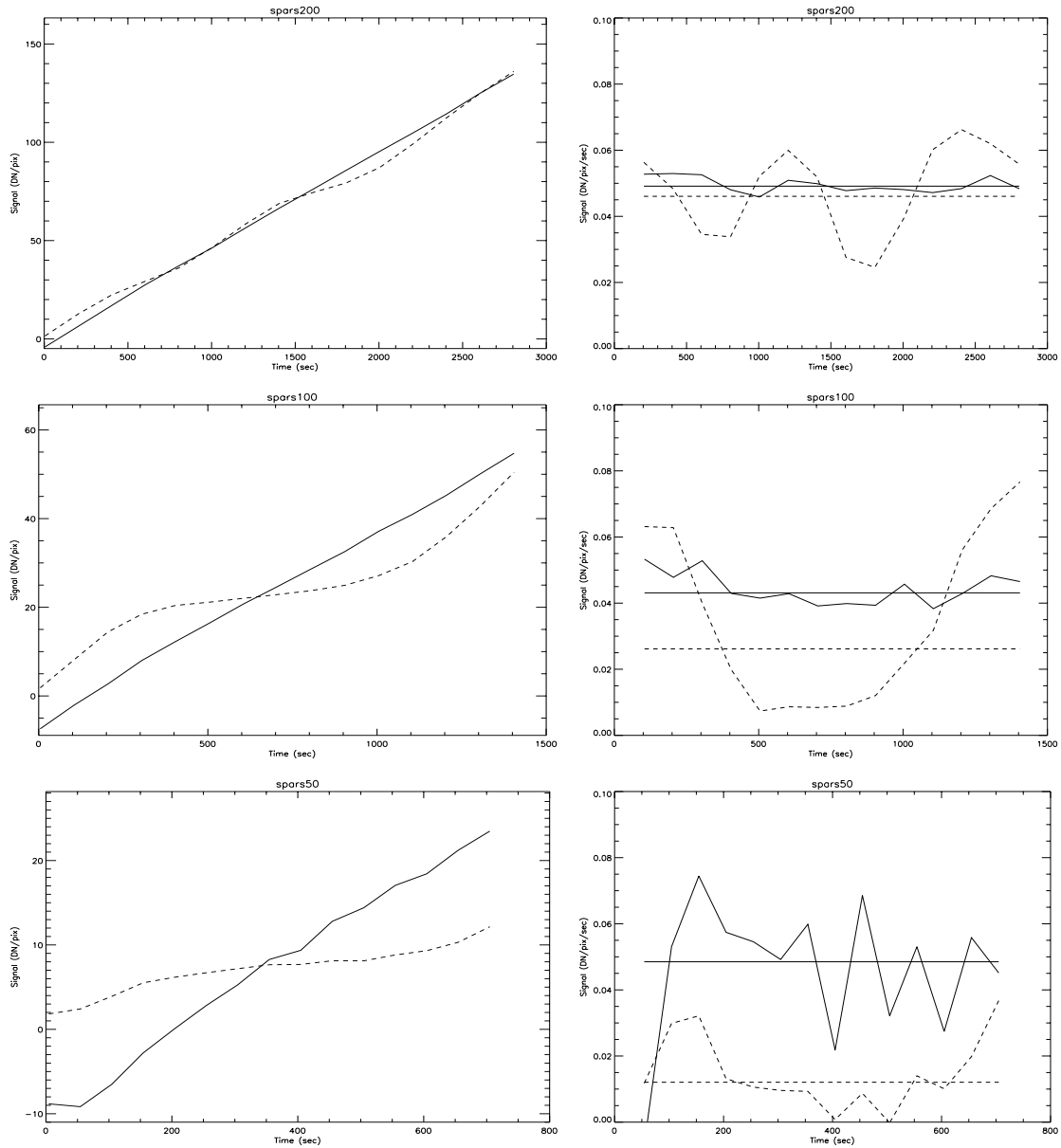


Figure 7: Results of the dark current calibration on a day 262 SPARS200 ramp, and day 251 SPARS100 and SPARS50 ramps (top to bottom). The panels on the left show the original quadrant-averaged signal (dashed line), and the corrected signals (solid line). The panels on the right show the effect of the correction in terms of dark rate. Again, the dashed line shows the original quadrant-averaged dark rate, while the solid line shows the corrected dark rate. The horizontal lines show the median dark rate up the ramp for the original file (dashed), and the corrected ramp (solid).

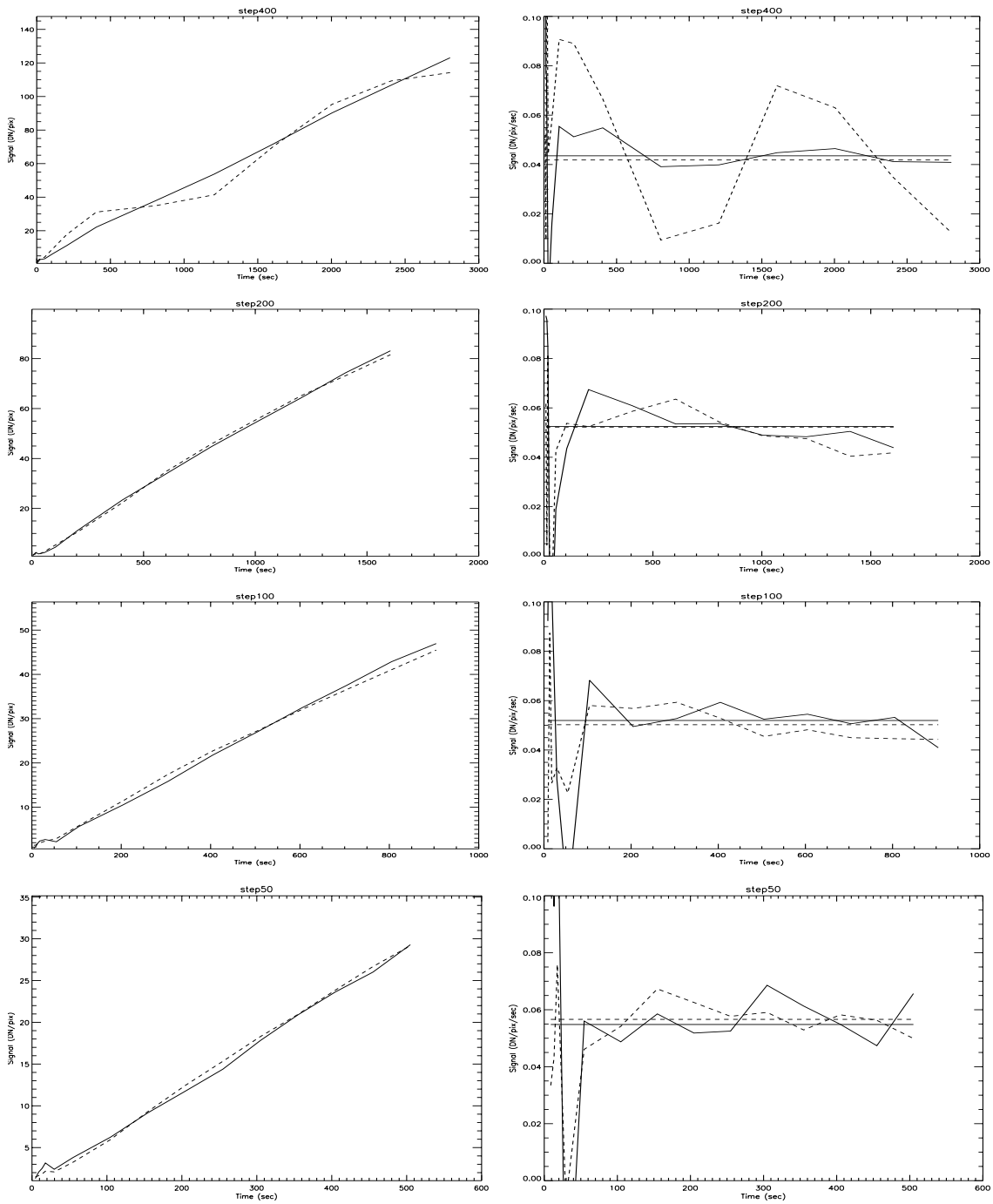


Figure 8: Same as Figure 7, but for the longer STEP sample sequences.

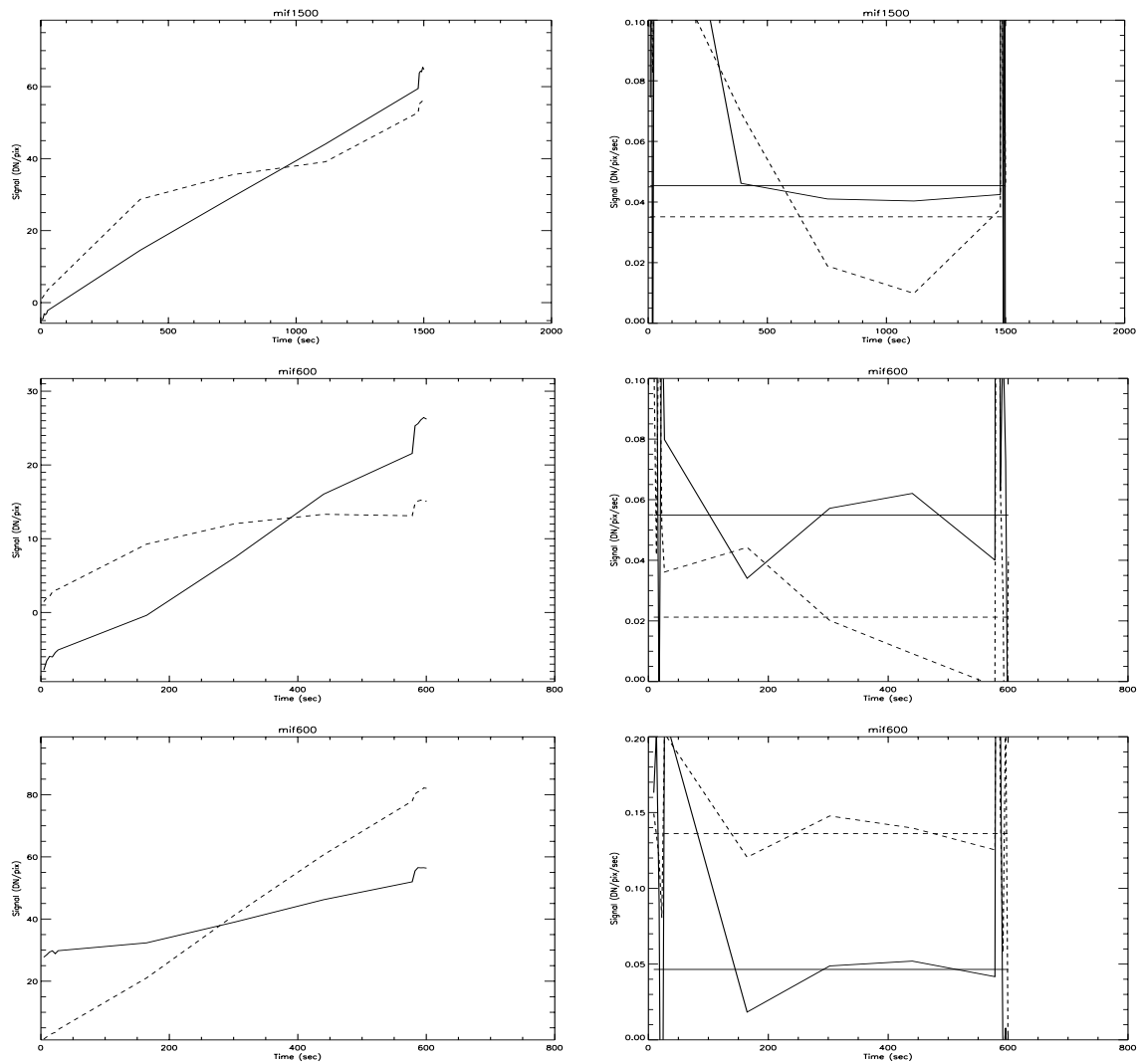


Figure 9: Same as Figure 7, but for the MIF1500 and MIF600 sample sequences. Note how the uncorrected quadrant-averaged rates for the two MIF600 ramps are below and above nominal, respectively. In both cases, the calibration returned the median signal to values close to the nominal dark rate.

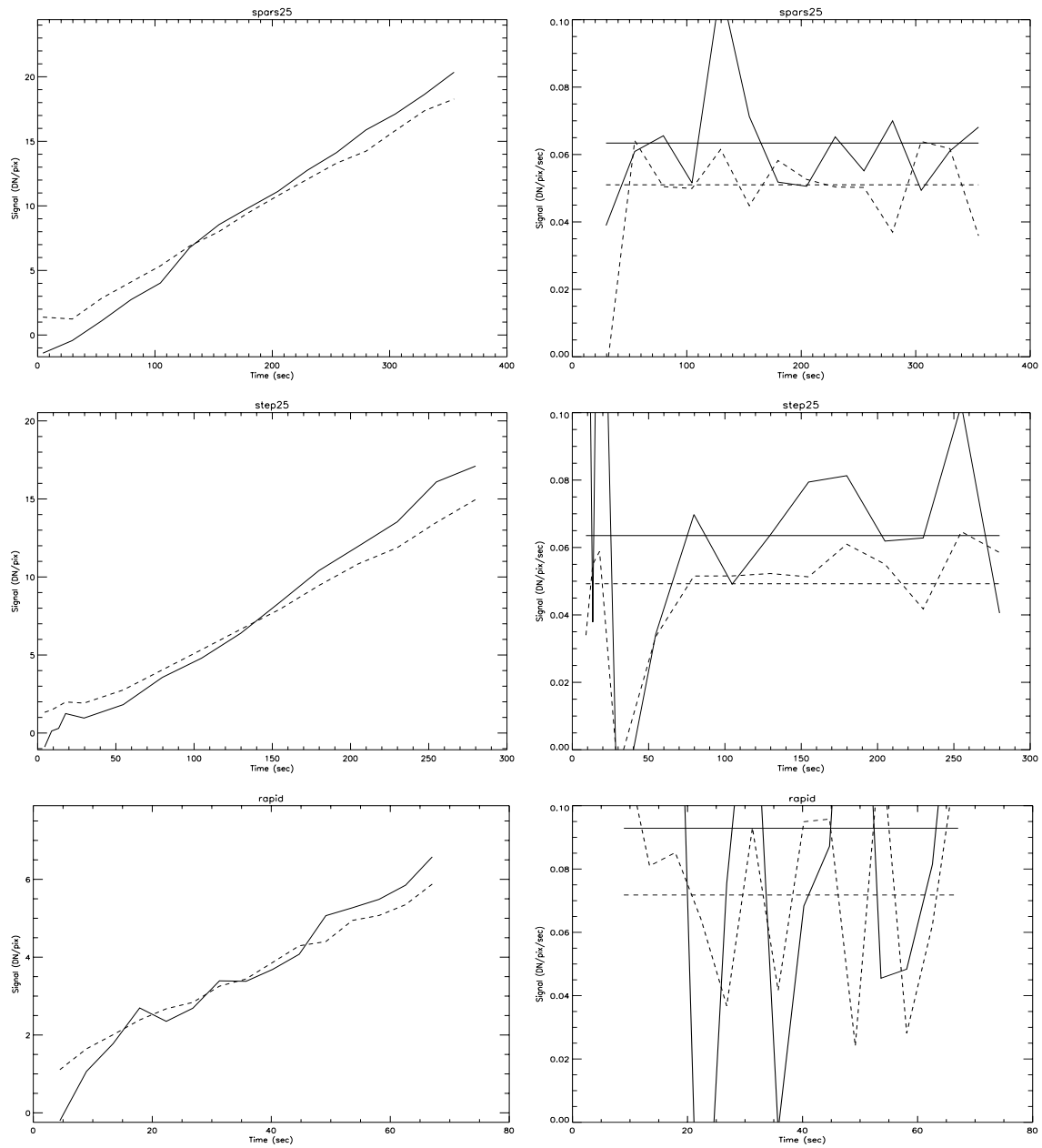


Figure 10: Same as Figure 7, but for the shortest sample sequences. In these cases, the dark current calibration appears to increase the noise of the signal up the ramp. In the case of the RAPID ramp in the bottom panels, the corrected signal appears to have a non-linearity to it that was not present in the uncorrected data.

Conclusions

The inboard reference pixels on FPA64 effectively track temperature-related variations in the dark current observed in the active pixels. These signal variations can be removed from WFC3-IR ramps by scaling the signal of the inboard reference pixels, and subtract-

ing this from the active pixels. The efficacy of this method decreases with the exposure time of the IR ramps. When applied to the STEP25, SPARS25, and RAPID ramps (280, 355, and 67 second exposure times, respectively), the correction increased the noise in the signal ramps and at times, appeared to make them less linear than before the correction was applied. An absolute calibration of the reference pixel behavior versus temperature may allow us to correct the shortest dark current ramps.

Recommendations

Integrate this correction into the standard pipeline processing for WFC3-IR.

References

Hilbert, B. and M. Robberto, **ISR 2005-25: WFC3-IR Thermal Vacuum Testing: IR Channel Dark Current.** 22 Aug 2005. <http://www.stsci.edu/hst/wfc3/documents/ISRs/WFC3-2005-25.pdf>

Hilbert, B., **ISR 2004-10: Basic IDL Data Reduction Algorithm for WFC3 IR and UVIS Channel.** 10 June 2004. <http://www.stsci.edu/hst/wfc3/documents/ISRs/WFC3-2004-10.pdf>

Robberto, M., **ISR 2002-06: The reference pixels on the WFC3 IR detectors.** 05 Jun 2002. <http://www.stsci.edu/hst/wfc3/documents/ISRs/WFC3-2002-06.pdf>